Journal of Quantitative Spectroscopy & Radiative Transfer 344 (2025) 109463

Contents lists available at ScienceDirect

Journal of Quantitative Spectroscopy and Radiative Transfer

journal homepage: www.elsevier.com/locate/jqsrt

Approaching experimental accuracy for triatomic spectra using variational calculations: Potential energy and dipole moment surfaces of $^{14}N_2{}^{16}O$

Irina I. Mizus [d], Mikhail A. Rogov [a,e], Nikolai F. Zobov [a], Vladimir Yu. Makhnev [c], Roman I. Ovsyannikov [a], Jonathan Tennyson [b], Oleg L. Polyansky [b,a,*]

[a] Institute of Applied Physics, Russian Academy of Sciences, 46 Ulyanov Street, Nizhny Novgorod, 603950, Russia
[b] Department of Physics and Astronomy, University College London, Gower Street, London WC1E 6BT, United Kingdom
[c] Center for Astrophysics, Harvard & Smithsonian, Cambridge, MA, USA
[d] Holon Institute of Technology, Golomb Street, 52, Holon, 5810201, Israel
[e] Department of Radiophysics, N. I. Lobachevsky State University of Nizhny Novgorod, 23 Gagarin Avenue, Nizhny Novgorod 603022, Russia

ARTICLE INFO

Keywords:
Variational calculations
Nitrous oxide
Rovibrational Schrödinger equation
Line intensities

ABSTRACT

The lower accuracy for line positions obtained using variational calculations (VCs) compared to effective Hamiltonian approaches is the main drawback in the VC methodology. The ability of VCs to make predictions for all the bands up to dissociation, treat several isotopologues at once and to incorporate first principle *ab initio* methods makes VCs the preferred method of constructing molecular line lists which are now widely used in astrophysics, planetary science and metrology. A significant step bringing VC of $^{14}N_2{}^{16}O$ line positions close to experimental accuracy is reported. High accuracy semi-empirical PESs are constructed by fitting to experimentally-derived rovibrational energy levels starting from available *ab initio* PESs. Three fitted PESs are presented, the best fit reproduces 279 energy levels up to 7000 cm^{-1} with $J = 0, 2$ and 5 with a standard deviation of 0.004 cm^{-1}, which drops to 0.0028 cm^{-1} when about 10 % of these levels (29 levels to be precise) are removed from the fit. The extrapolation to higher J quantum numbers is shown to be very accurate up to $J = 15$. For extrapolation to higher J values, an additional fit of higher J energy levels is conducted, which results in a standard deviation of 0.005 cm^{-1} for 535 energy levels with $J = 0, 2, 5, 10$, and 15. An *ab initio* dipole moment surface is computed and used to produce transition intensities in good agreement with the observations.

1. Introduction

There are two major methodologies for calculating molecular rotation-vibration energy levels and hence rovibrational line centres: effective Hamiltonians which are generally based on the use of perturbation theory and variational calculations which use the variational principle. There are many advantages to variational calculations including both the ability to give complete line lists [1] and the ability to transfer spectroscopic models between isotopologues [2], which is why the molecular line lists used in a variety of applications such as astrophysics, atmospheric monitoring and metrology, are increasingly being calculated using the variational approach [3]. However, there is one serious disadvantage to this approach. Effective Hamiltonians are often capable of delivering experimental accuracy for energy levels calculations, especially when the molecular system is semi-rigid and not floppy with not too many resonances. While effective Hamiltonian approaches are capable of reproducing line position with experimental accuracy, variationally calculated line centres do not yet approach this accuracy.

One approach to increasing the accuracy of variational calculations is to fit the molecular potential energy surface (PES) using experimentally derived values of the rovibrational energy levels (or directly to transitions). In cases when the Born–Oppenheimer approximation works well and the nuclear motion kinetic energy used is exact within the Born–Oppenheimer approximation, this approach in principle should provide high accuracy. Variational approaches rely on the use of basis functions to converge the energy levels with the critical step often being diagonalization of the Hamiltonian matrix. Modern computers allow the use of very large matrices, so that numerical solution of the nuclear-motion Schrödinger equation can be obtained very accurately for many energy levels using the Macdonald theorem [4] which states that increasing the basis set size (and hence the size of the Hamiltonian matrix) leads to monotonically better convergence

* Corresponding author.
E-mail address: o.polyansky@ucl.ac.uk (O.L. Polyansky).

https://doi.org/10.1016/j.jqsrt.2025.109463
Received 18 July 2024; Received in revised form 31 March 2025; Accepted 31 March 2025
Available online 14 May 2025

towards the exact solution of the Schrödinger equation for all bound levels. In particular the convergence of 10^{-2} to 10^{-3} cm^{-1} is the typical convergence achieved for the fitting of the PESs [5,6]. Even higher convergence has been achieved for vibration–rotation calculations on H_3^+ [7–9]. Thus, when a PES is fitted to empirical energy levels, all the components are in place to achieve the desired accuracy.

The accuracy of the calculated line centres can be characterized by the standard deviation (σ) with which the observed energy levels are reproduced. Due to the effects of the Born–Oppenheimer approximation, the reality of computations of molecular line lists for polyatomic molecules can be divided between hydrogen containing molecules and heavier systems. For H-containing species, for which water, H_2O and hydrogen cyanide, HCN, are the two most studied examples, For both water and HCN, the best values of the standard deviations achieved are $\sigma = 0.012$ cm^{-1} [6,10]. Estimates suggest that this limit is likely due to the yet unsolved non-adiabatic problem and attempts to further lower σ will require a better treatment of non-adiabatic effects. Possible ways to do this are described in Refs. [11–13].

Turning to heavier molecules, which do not contain H atoms, important triatomic example include CO_2, O_3, and N_2O. It appears that influence of Born–Oppenheimer breakdown on the accuracy of the calculated energy levels is about an order of magnitude smaller than for water or HCN [14]. As a result, one might expect significantly higher accuracy calculations using semi-empirical, fitted PESs for these important molecules. However, so far this has not been the case: the best standard deviations achieved about 0.02 cm^{-1} for CO_2 [15,16] and 0.025 cm^{-1} for O_3 [17,18]. Up until recently there was no accurately fitted PES for N_2O. Huang et al. recently published a computed $^{14}N_2{}^{16}O$ line list based on a fitted PES [19]. Comparing their energy levels to the set of empirical levels used in our fits below suggests that Huang et al. fitted PES results in a standard deviation of 0.038 cm^{-1}; the recent ExoMol line list [20] is generated using a PES which gives a somewhat higher standard deviation. It would seem therefore that σ for all these published PESs of the non-H containing molecules are counter-intuitively several times higher then those obtained for H_2O and HCN. The goal of the present work is to obtain a fitted PES for $^{14}N_2{}^{16}O$ which reduces σ from 0.03 cm^{-1} towards the experimental accuracy of around 10^{-3} cm^{-1}. In this paper we are able to achieve a σ approaching 0.0028 cm^{-1}, which is close to the average experimental accuracy (about 0.001 cm^{-1}) as documented by the recent MARVEL (measured active rotation-vibration energy levels) study on N_2O [21].

The motivation of our study was not only to significantly improve the accuracy of variationally calculated $^{14}N_2{}^{16}O$ line positions, but also to produce the basis for constructing a high accuracy, high temperature $^{14}N_2{}^{16}O$ line list which requires both an accurate fitted PES and a high quality dipole moment surface (DMS). Until the recent work of Huang et al. [19], which appeared after we had started this project, there has been no accurate variationally-calculated line list of this important molecule (the fourth most important atmospheric molecule in the HITRAN [22]). Huang's et al. work motivated us to seek further improvements in the accuracy of our calculations. We note that Tashkun and Campargue have also recently provided a room temperature $^{14}N_2{}^{16}O$ line list in the NOSL-296 database [23] which was computed using the effective Hamiltonian approach and improved on the earlier NOSD-1000 database [24].

$^{14}N_2{}^{16}O$ energy levels of accuracy approaching experimental are needed for two major purposes. First, we need them to benchmark the calculated energy levels. Second, when all our efforts result in calculated line list for modelling spectra at arbitrary temperatures, using the experimentally accurate energy levels (when known) to substitute the calculated ones could result in much more accurate knowledge of the line positions of the line list than what we had as a result of purely theoretical efforts. The possibility to obtain such levels is provided by the so-called MARVELisation procedure, which uses the program MARVEL [25] to derive the experimentally accurate molecular energy levels.

There are continuing experimental efforts to elucidate the high resolution spectrum of N_2O with at least fifteen studies in the last five years alone [26–40]. A review of all high resolution studies and an assigned set of validated energy levels are provided in the recent MARVEL study on N_2O [21]. The empirical energy levels derived in this study are used in the current work.

Another major reason for needing an accurate fitted PES is to calculate accurate line intensities set, which is best done, using a fitted PES and an *ab initio* DMS. Line intensities can be predicted using this technique to better than 0.1% [41,42]; however, we have shown [6] that the difference in intensities calculated using the same DMS and two different seemingly accurate PESs with $\sigma = 0.012$ cm^{-1} and 0.027 cm^{-1} give accuracies which vary between the PESs by between 0.1 to 0.5% for about quarter of the calculated lines. This is a large difference when compared with an accuracy requirement of 0.1%; this emphasizes the need for highly accurate PESs. Thus, at the same time with working on improvement of the fitted PES, we also calculate an *ab initio* DMS and present $^{14}N_2{}^{16}O$ line intensity calculations using different PESs and DMSs.

Line positions of $^{14}N_2{}^{16}O$ have long been measured to high accuracy [43–46] and such studies are continuing today [47,48]; a complete review of experimental high resolution rotation-vibration $^{14}N_2{}^{16}O$ spectra has recently been given by Tennyson et al. [21]. However, there has been far less emphasis on obtaining high accuracy, sub-percent, transition intensities. An accuracy of 3 to 5 percent used to be standard for many years and many measurements are available at this level of accuracy. Recently, line intensities for several $^{14}N_2{}^{16}O$ bands have been measured with the sub-percent accuracy [49–52]. Two of these studies [49,50] used lasers for the intensity measurements, which increases somewhat the accuracy of the line intensity determination. Specifically, Adkins et al. [50] observed the (4200)←(0000) and (5000)←(0000) bands near 1.6 μm and obtained a nominal combined standard uncertainty for the intensities of 1 % for most lines. Odinsova et al. [49] studied eight $^{14}N_2{}^{16}O$ transitions, mainly belonging to the P-branch of the $3\nu_1 + 2\nu_2$ vibrational band obtaining an experimental uncertainty of about 0.4%. While Karlovets et al. [51] observed 47 bands belonging to the $^{14}N_2{}^{16}O$, $^{14}N^{15}N^{16}O$, $^{15}N^{14}N^{16}O$ and $^{14}N_2{}^{18}O$ isotopologues with intensities estimated to be accurate to 3 % or better for most lines but up to 20 % for the weakest or strongly blended lines. Subsequently, Karlovets et al. [52] have presented a further 49 bands with the same uncertainties. These measurements are of crucial importance for obtaining of accurate variationally-calculated line lists, as comparison of the calculated values with the experimental ones can be used to characterize the quality of the calculations. These calculations are required in many applications such as monitoring the Earth atmosphere and analysis of exoplanetary atmospheres. In particular, it has been suggested that N_2O should be an observable species in the atmospheres of Earth-like exoplanets [53] where it may be a possible bio-signature [54]. As a result, N_2O features on the list of target species in exoplanet characterization missions [55,56].

This paper is organized as follows. In Section 2 we describe the calculation of the fitted PES, which is needed for the accurate wavefunctions. Also further improvement of the line positions via MARVELisation procedure of $^{14}N_2{}^{16}O$ is described. In Section 3 we present the $^{14}N_2{}^{16}O$ intensity calculations and extensively compare these results with the experimental values, focusing on the sub-percent accurate experiment and conclusions are outlined in Section 4.

2. Potential energy surface

There are three major requirements for high accuracy *ab initio* intensity calculations: (1) an accurate program for the solution of the ro-vibrational Schrödinger equation such as DVR3D [57]; (2) an accurate potential energy surface (PES), which in practice is obtained starting from an *ab initio* PES which is modified by fitting to experimentally-derived ro-vibrational energy levels and (3) an accurate, usually purely

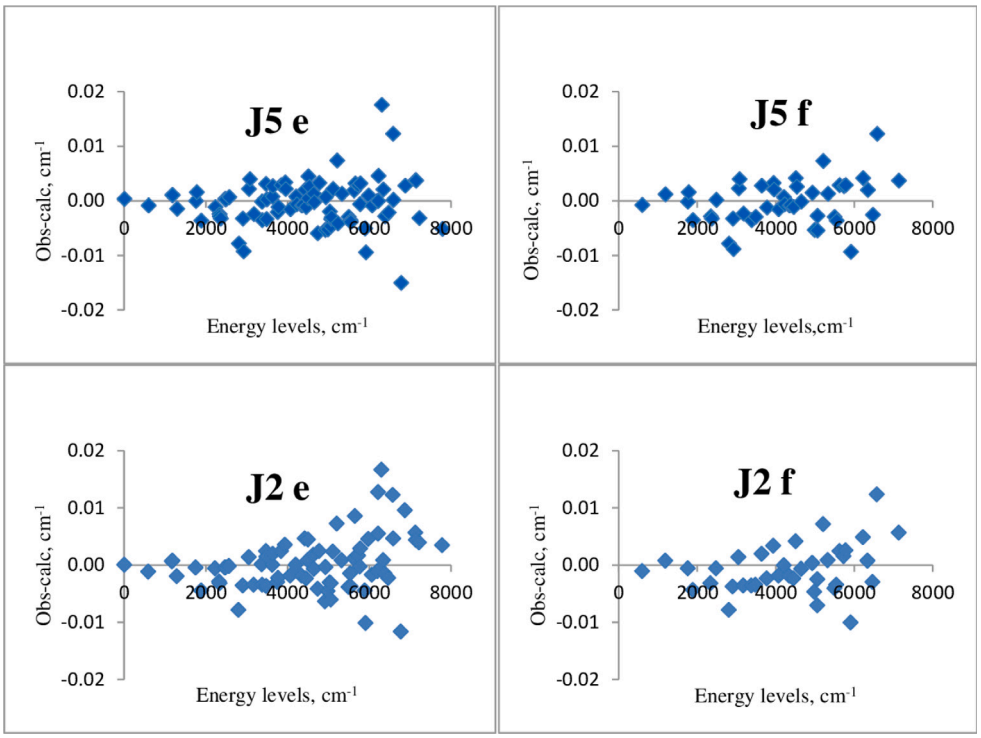

Fig. 1. Difference between experimental and calculated (PES60) energy levels for $J = 2, 5$.

ab initio, dipole moment surface (DMS). In this section we deal with the PES part.

Until recently there were only two available ground state PESs for N_2O, neither of which could be used to give precise models of the spectrum. The oldest PES by Zuniga et al. from 1996 [58] was empirically fitted with the accuracy of a few tens of wavenumbers for higher vibrational states. More recently, Schröder et al. [59] constructed a high level *ab initio* PES. Discrepancies between the experimentally derived energy levels and the *ab initio* rovibrational energy levels are only a few cm^{-1}, see Table 3 of Ref. [59]. This accuracy is very far away from the experimental one of about 10^{-3} cm^{-1}. This kind of accuracy is necessary for a variety of purposes — accurate modelling of the spectrum with the correct line centres, production of the accurate wavefuntions for the accurate line intensity calculations.

In order to obtain an accurate PES, the PES is refined to fit experimentally-derived energy levels [5,60]. The fitting of the $^{14}N_2{}^{16}O$ PES and the results of this fit are described in Section 2.3. First, in the following subsection, we present the results of the energy levels calculation using the *ab initio* PES [59].

2.1. Ab initio PES

The *ab initio* PES of Schröder et al. [59] was obtained using a highly sophisticated level of theory. In particular, a composite approach with the basic contribution given by explicitly correlated coupled-cluster (CC) calculations was used. Smaller contributions include corrections due to inner-shell correlation, scalar-relativistic effects and higher-order correlation up to iterative pentuple excitations (CCSDTQP in CC nomenclature). The importance of higher-order correlation for reaching the desired accuracy led to the use of an extrapolation scheme to approximately account for the effect of hextuple and some pentuple excitations (see Fig. 2).

Schröder et al. [59] used their PES to calculate $J = 0$ energy levels using their own program to solve the nuclear-motion Schrödinger equation. These levels and their obs.-calc. values are given in the Table 1, columns "Obs." and "Obs.-Calc. Schröder", respectively. We use this PES as a starting point for the fit of the PES to the experimental energy levels values within the framework of our open-source[1] rovibrational program DVR3D [57].

For the DVR3D [57] calculations we used the Jacobi coordinates to represent the kinetic energy operator and z-axis embedded along the r_1 one (parameter ZEMBED = F [57]). Initial calculations used Morse oscillator-like functions for both radial coordinates but these proved to be non-variational for reasons that have been identified previously [61]. The results reported here all used spherical oscillator functions for the scattering coordinate. For the diatomic (outer $N - O$) coordinate we use a discrete variable representation (DVR) grid based on Morse-like oscillator functions with parameters $r_e = 4.5$, $D_e = 0.2$, and $\omega_e = 0.01$ in atomic units and spherical oscillator with parameters 0.0, 0.0 and 0.25 for the scattering coordinate [57]. For the fits we used 60, 50, and 60 grid points for two radial and the angular scattering coordinates, respectively, while calculating eigenvalues with the total angular momentum quantum number values $J = 0$ and 2, and 60, 60, and 60 grid points for $J = 5$, and a final Hamiltonian matrix dimension for solving the vibrational problem equal to 10 000. As is usual for DVR calculations most of these calculations were performed using the quadrature approximation for most of the matrix elements; however, after tests, this approximation not used for the scattering coordinate which goes to zero for linear NNO geometries; see Ref. [61] for a discussion of this issue.

We recalculated the $J = 0$ levels using the *ab initio* PES of [59] using DVR3D. The results of these calculations are given in the Table 1 which shows very good agreement with the more limited in scope original calculations. While this is not an ultimate proof of the optimal choice of parameters for our calculations, the eventual excellent result of the fit (see below) indicates that the parameters we are using are good enough to allow us to achieve the improvement in the accuracy of the energy levels.

[1] https://github.com/exomol/DVR3D.

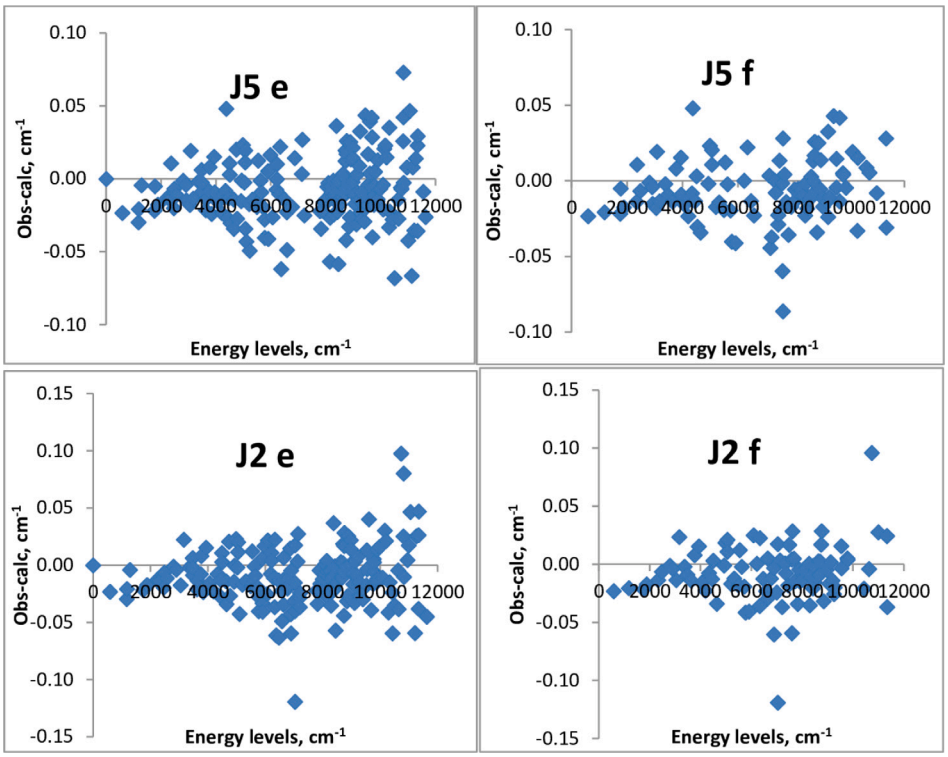

Fig. 2. Difference between experimental and calculated (PES12) energy levels for $J = 2, 5$.

2.2. Empirical energy levels using MARVEL

We consider levels with $J = 0$ up to 7000 cm^{-1}.

There are two major reasons why we concentrate on the energies in the limited range. First, we are interested in the fitting the PES to obtain energy levels as close to experiment as possible; in the fact the PES produces not only the energies via solution of the Schrodinger equation, but also the corresponding wavefunctions. These wavefunctions can subsequently be used to calculate the line intensities. Since the MARVELisation procedure described below, helps to obtain the line positions close to experimentally accurate ones, we could have dropped the quest for as accurate PES as possible and rely entirely on the MARVELisation of the energy levels used. However, the use of the wavefunctions produced using the fitted PES for intensity calculations makes the goal of accurately fitting the PES extremely important. A goal of the line intensity calculations is the subsequent comparison of them with the experimentally observed ones. This comparison validates the use of the calculated line intensities beyond the ones, observed experimentally. This is needed because the experiment is always limited for obvious reasons and calculations are capable of providing important line intensities for hundreds and thousands more lines than are available experimentally. In particular, extrapolation to higher temperatures than those readily accessible experimentally is easily available to the calculations [1]. As modern experiments which determine transition intensities with sub-percent accuracy are mostly available for the lines which lie below 7000 cm^{-1}, it was natural to concentrate on this lower energy range. Second, fitting all available energies, potentially up to dissociation, in one go significantly reduces the accuracy of the fit and the corresponding wavefuctions. The accuracy of the calculated intensities is therefore compromised. However, for many applications completeness of the range of the PES is more important than its accuracy. For that reason we decided to also construct a PES valid up to 12 000 cm^{-1} (see the end of Section 2.4.3) .

In the fit we used 118 MARVEL levels in the range 0–7000 cm^{-1}, and 91 levels from HITRAN database. When the level is present in both sets (MARVEL and HITRAN) the difference between them is less than 0.001 cm^{-1} with a single exception of $J = 2e$ (21^10) level 3168.313 cm^{-1}. Up to about 4000 cm^{-1} all experimental levels are present in both sets. Higher in energy about 40% of the levels are present only in one of the sets, the remaining in both. The differences are still less than 0.001 cm^{-1}. The number of calculated levels in the region is 265. The G_v analogue of $J = 0$ levels for all vibrational states with $l \neq 0$ have not been used here.

2.3. Fit of the PES starting from ab initio PES

The typical accuracy of the majority of the empirically-determined energy levels is about 10^{-3} cm^{-1}. Such accuracy of the rovibrational energy level calculations using variational approach could be achieved at present only for diatomic molecules. For triatomic molecules the best accuracy reached yet is about 10^{-2} cm^{-1} [6] for water spectra up to 15 000 cm^{-1}. For the molecules with heavier atoms, like ozone and carbon dioxide, the best accuracy reached is about 0.03 cm^{-1}. This is approximately the accuracy of the energy levels computed by Huang et al. for N_2O [19].

In order to fit the PES we use the DVR3D [57] program suite. As practically every fit of the PES within the variational approach is done nowadays (since 1997, when Partridge and Schwenke fitted the water PES [62] starting from the multi-reference configuration interaction (MRCI) PES, calculated *ab initio*) we started our $^{14}N_2{}^{16}O$ PES fit with the *ab initio* surface due to Schröder et al. [59], with the PES given by the formula

$$V - V^e = \sum_{k,m,n=0}^{k+m+n=8} C_{kmn}(r_{NN} - r^e_{NN})^k (r_{NO} - r^e_{NO})^m (\theta_e - \theta)^n, \qquad (1)$$

where C_{kmn} is a set of 52 (excluding the free term $C_{000} = V^e$ of the polynomial) empirically determined coefficients; k, m and n are the integer numbers (n must be even); r_{ij} — the bond length between atoms i and j, r^e_{ij} — the bond equilibrium length between atoms i and j, θ and $\theta_e = \pi$ — instantaneous and equilibrium bond angles, respectively. This analytical form of the potential is identical to the one used by Schröder to represent his PES. During the fitting procedure, we vary the initial

Table 1
Vibrational band origins ($J = 0$ levels), taken from [58], in cm^{-1}: comparison of our DVR3D calculations with the calculations due to Schröder et al. [59] using Schröder et al.'s *ab initio* PES.

v_1, v_2^0, v_3	Obs.	Obs.-Calc. DVR3D	Obs.-Calc. Schröder
0 2 0	1168.13	−0.07	−0.07
1 0 0	1284.90	−0.42	−0.42
0 0 1	2223.76	−0.19	−0.19
0 4 0	2322.57	−0.07	−0.07
1 2 0	2462.00	−0.59	−0.59
2 0 0	2563.34	−0.88	−0.88
0 2 1	3363.98	−0.44	−0.44
0 6 0	3466.60	−0.01	−0.01
1 0 1	3480.82	−0.64	−0.63
1 4 0	3620.94	−0.73	−0.73
2 2 0	3748.25	−1.16	−1.16
3 0 0	3836.37	−1.41	−1.41
0 0 2	4417.38	−0.30	−0.27
0 4 1	4491.54	−0.63	
1 2 1	4630.16	−0.97	
2 0 1	4730.82	−1.14	
1 6 0	4767.14	−0.82	
2 4 0	4910.99	−1.40	
3 2 0	5026.30	−1.73	
4 0 0	5105.68	−2.07	
0 2 2	5529.70	−0.78	
1 0 2	5646.74	−0.75	
1 4 1	5762.37	−1.25	
2 2 1	5888.10	−1.52	
3 0 1	5974.84	−1.75	
3 4 0	6192.27	−2.04	
4 2 0	6295.45	−2.29	
5 0 0	6373.31	−2.88	
0 0 3	6580.86	−0.33	
0 4 2	6630.41	−1.22	
1 2 2	6768.48	−1.28	
2 0 2	6868.53	−1.30	
2 4 1	7024.07	−1.83	
3 2 1	7137.10	−2.04	
4 0 1	7214.65	−2.52	
4 4 0	7463.96	−2.59	
5 2 0	7556.11	−2.88	
6 0 0	7640.45	−3.77	
0 2 3	7665.22	−1.16	
1 0 3	7782.64	−0.78	
1 4 2	7873.50	−2.40	
2 2 2	7998.56	−1.83	
3 0 2	8083.93	−2.00	
3 4 1	8276.30	−2.43	
4 2 1	8376.32	−2.56	
5 0 1	8452.61	−3.46	
0 0 4	8714.12	−0.25	
1 2 3	8877.03	−1.58	
2 0 3	8976.50	−1.33	
2 4 2	9108.39	−2.24	
3 2 2	9219.04	−2.26	
4 0 2	9294.97	−2.88	
4 4 1	9517.92	−2.74	
5 2 1	9606.31	−3.11	
1 0 4	9888.58	−0.63	
2 2 3	10 079.56	−2.04	
3 0 3	10 163.61	−2.02	
4 2 2	10 429.12	−2.69	
0 4 4	10 815.27	−0.74	
0 0 5	10 820.14	−1.66	
0 2 5	11 844.97	−1.69	
1 0 5	11 964.25	−0.61	
0 0 6	12 891.15	−0.59	
1 0 6	14 009.69	−0.98	
0 0 7	14 934.27	−2.23	

set of C_{kmn} in the way that allows us to minimize the standard deviation between the resulting energy levels and the experimental data set.

There are 279 empirical energy levels (both the MARVEL ones and the levels from the HITRAN database) with $J = 0, 2$ and 5 which lie to about 7000 cm^{-1}; these formed the basis for our fits. After a significant number of trials we managed to obtain PES53, which gives an accuracy of 0.0089 cm^{-1} for the whole set of 0, 2 and 5 experimental energy levels.

We then attempted to further improve the accuracy by increasing the number of polynomial parameters C_{kmn} from the original 53 terms used to represent Schröder's PES. First, we increased the expansion to 60 terms obtaining a new PES60, and then considered the whole set of 96 polynomial terms which satisfy $k + m + n \leq 8$ giving PES96. The standard deviations, obtained for the set of experimental energy levels up to 7000 cm^{-1} for calculations with the new PES60 and PES96, are 0.0054 cm^{-1} and 0.0041 cm^{-1}, respectively.

In an attempt to get the most accurate wavefunctions for some of the vibrational states, we also removed about 10% of the levels which gave the highest residues. The resulting fits with partial sets of experimental data we called PES60a and PES96a. The standard deviations of these fits were 0.0032 cm^{-1} with PES60a for a set of 251 energy levels and 0.0028 cm^{-1} with PES96a for a set of 250 energy levels. We present a comparison of the experimental and calculated $J = 0$ levels for all 5 obtained variants in the Table 2.

Prediction of band origins ($J = 0$ levels) between 7000 and 15 000 cm^{-1} with the potentials obtained are given in the Table 3.

All our PESs are given as supplementary material to this work.

2.4. Final results of the fit and extrapolation results

We decided to present all three PESs obtained, that is PES53, PES60 and PES96, as each of them have their own advantages. The standard deviation of the 279 $J = 0, 2$ and 5 fitted levels as well as the results with the removal of about 10% of the levels from the fit are given in the Table 4. The level-by-level list of residues (observed minus calculated values), which were used while calculating standard deviation values performed in the Table 4, is presented in the Supplementary material, Table 2.

In particular, PES53 was the first one, which resulted in a significant improvement of the σ from the *ab initio* value of 0.04 cm^{-1}. This surface's peculiarity is that we did not change the number of parameters from the original Schröder et al. number of constants $N = 53$. We fitted only these 53 original constants. The second major improvement by about two times happened when we added 7 parameters to obtain PES60 – σ became 0.005 cm^{-1}. The final PES used to fit levels up to 7000 cm^{-1} was PES96. We added 36 parameters but the improvement was only marginal. The advantage of this PES is that it is still the most accurate but the disadvantage is that this minor improvement was obtained using a significant increase in the number of constants. This PES demonstrates that a further increase of the number of constants will not be productive and if we want to further lower σ, making it closer to experimental accuracy, we need a significant improvement in the present theory (see Conclusions below).

In order to better characterize the results obtained using the above PESs we present the standard deviations for a set of the reliable MARVELised energy levels of $^{14}N_2{}^{16}O$ only. These levels are based purely on the experimental values. The possibility of the problematic levels in a MARVELised set comes from the situations where a level is determined from the only one line position, and this line is misassigned. Otherwise the MARVELised levels have even higher accuracy than the experimental accuracy, as they are obtained by the averaging of the information from the different line positions, which contain the level in question.

Table 5 shows that for all the sets of data used and all the Js, the standard deviations are practically equal to the ones given in much less detailed Table 4, where σ is only presented for the levels which we actually fitted. Thus, the results shown in Table 5 confirm the high accuracy of the PESs obtained. The level-by-level list of residues, which were used while calculating σ values performed in the Table 5, is presented in the Supplementary material, Table 3.

Table 2
Fitted and predicted levels, in cm^{-1}, calculated with PES53, PES60, PES96, PES60a, PES96a, PES60hJ and PES12 with $J = 0$.

v_1, v_2, v_3	Obs.	Obs.-Calc. PES53	Obs.-Calc. PES60	Obs.-Calc. PES96	Obs.-Calc. PES60a	Obs.-Calc. PES96a	Obs.-Calc. PES60hJ	Obs.-Calc. PES12
0 2 0	1168.132	−0.007	−0.002	0.003	0.001	0.001	0.003	−0.030
1 0 0	1284.903	−0.013	−0.007	−0.003	−0.003	−0.002	−0.006	−0.004
0 0 1	2223.757	−0.014	−0.004	0.002	−0.001	−0.001	0.002	−0.013
0 4 0	2322.573	−0.010	−0.003	−0.001	0.000	−0.003	0.002	−0.013
1 2 0	2461.996	−0.010	−0.007	−0.001	−0.003	−0.001	−0.005	−0.020
2 0 0	2563.339	−0.013	−0.004	0.001	−0.002	−0.000	−0.004	−0.011
0 2 1	3363.978	−0.008	−0.001	0.002	−0.002	0.000	0.001	−0.002
0 6 0	3466.600	−0.011	−0.004	0.003	0.000	0.002	0.001	0.007
1 0 1	3480.819	−0.003	0.004	0.004	0.005	0.001	0.002	−0.002
1 4 0	3620.943	−0.006	−0.002	0.000	0.001	−0.000	0.001	−0.021
2 2 0	3748.252	−0.013	−0.010	−0.004	−0.005	−0.003	−0.008	−0.008
3 0 0	3836.371	−0.007	0.002	0.004	0.003	0.002	−0.002	−0.023
0 0 2	4417.378	−0.005	0.001	0.006	0.005	0.005	0.005	−0.027
0 4 1	4491.542	−0.005	0.000	0.001	0.002	0.001	0.003	0.011
1 2 1	4630.161	−0.004	−0.002	0.003	−0.002	0.002	−0.002	−0.014
2 0 1	4730.825	−0.010	−0.007	−0.004	−0.001	−0.004	−0.006	0.021
1 6 0	4767.142	−0.004	0.002	0.004	0.005	0.002	0.005	−0.027
2 4 0	4910.995	−0.013	−0.009	−0.007	−0.004	−0.006	−0.007	−0.014
3 2 0	5026.303	−0.013	−0.009	−0.007	0.001	−0.003	−0.009	−0.002
4 0 0	5105.677	−0.005	0.001	0.002	0.004	0.002	−0.006	−0.042
0 2 2	5529.695	−0.006	0.000	0.004	−0.000	−0.002	0.002	−0.016
1 0 2	5646.740	0.004	0.009	0.010	0.008[a]	0.009[a]	0.009	−0.009
1 4 1	5762.373	−0.015	−0.008	−0.001	−0.004	−0.000	−0.002	−0.028
2 2 1	5888.106	−0.009	−0.008	−0.003	−0.004	−0.005	−0.008	0.006
3 0 1	5974.845	−0.008	−0.007	0.003	0.003	0.004	−0.005	0.017
2 6 0	6058.667	−0.008	−0.004	−0.001	−0.001	−0.002	−0.007	−0.025
3 4 0	6192.271	−0.012	−0.008	−0.005	−0.001	−0.001	−0.011	−0.006
4 2 0	6295.448	0.005	0.006	0.006	0.024[a]	0.016[a]	0.003	−0.009
5 0 0	6373.308	−0.008	−0.007	−0.005	−0.002	−0.002	−0.011	−0.061
0 0 3	6580.854	0.006	0.006	0.004	0.005[a]	0.005[a]	0.007	−0.049
1 2 2	6768.502	−0.015	−0.006	−0.002	−0.008[a]	−0.01[a]	−0.009	−0.019
2 0 2	6868.550	0.012	0.013	0.011	0.021[a]	0.009[a]	0.000	0.015
3 2 1	7137.127	0.011	0.011	0.006	0.008	0.004	0.007	0.027
4 0 1	7214.680	−0.011	−0.005	0.001	0.001	0.004	−0.011	−0.024
1 0 3	7782.662	−0.009	−0.002	0.005	−0.009	0.003	−0.007	−0.022

[a] Designate levels not included in the fit.

Table 3
Fitted and predicted levels, in cm^{-1}, calculated with PES53, PES60, PES96, PES60a, PES96a, PES60hJ and PES12 with $J = 0$.

v_1, v_2, v_3	Obs.	Obs.-Calc. PES53	Obs.-Calc. PES60	Obs.-Calc. PES96	Obs.-Calc. PES60a	Obs.-Calc. PES96a	Obs.-Calc. PES60hJ	Obs.-Calc. PES12
2 2 2	7 998.589	0.002	−0.022	0.004	−0.042	−0.024	−0.0530	−0.017
3 0 2	8 083.953	−0.017	−0.027	−0.010	−0.034	−0.060	−0.0834	0.002
4 2 1	8 376.326	0.008	−0.006	−0.046	−0.010	−0.013	−0.0186	0.037
5 0 1	8 452.636	−0.036	−0.078	−0.053	−0.083	−0.075	−0.1014	−0.057
0 0 4	8 714.140	0.052	0.036	0.045	0.034	0.035	0.0154	0.019
1 2 3	8 877.042	−0.094	−0.091	−0.099	−0.120	−0.117	−0.1286	−0.027
2 0 3	8 976.489	−0.070	−0.069	−0.075	−0.079	−0.134	−0.1225	0.021
2 4 2	9 108.322	−0.109	−0.157	−0.108	−0.185	−0.138	−0.0700	−0.029
3 2 2	9 219.040	−0.129	−0.190	−0.184	−0.227	−0.215	−0.2153	0.010
4 0 2	9 294.994	−0.218	−0.273	−0.246	−0.294	−0.323	−0.3471	−0.027
4 4 1	9 517.874	−0.076	−0.115	−0.198	−0.118	−0.138	−0.0920	−0.017
5 2 1	9 606.336	−0.063	−0.077	−0.246	−0.088	−0.117	−0.1430	0.039
1 0 4	9 888.58[a]	−0.064	−0.037	−0.087	−0.043	−0.102	−0.1021	0.000
2 2 3	10 079.556	−0.330	−0.380	−0.363	−0.435	−0.447	−0.4434	0.005
3 0 3	10 163.593	−0.477	−0.492	−0.534	−0.522	−0.643	−0.6256	0.035
4 2 2	10 429.151	−0.680	−0.746	−0.923	−0.815	−0.840	−0.8713	−0.012
0 0 5	10 815.251	0.140	0.091	0.119	0.021	0.064	0.0825	0.014
0 4 4	10 820.128	−0.224	−0.151	−0.197	−0.201	−0.188	−0.1757	0.084
0 2 5	11 844.97[a]	−0.115	−0.154	−0.125	−0.257	−0.247	−0.2473	0.057
1 0 5	11 964.122	−0.844	−0.754	−0.905	−0.769	−0.996	−0.8684	0.056
0 0 6	12 891.079	−0.792	−0.824	−0.757	−0.838	−1.011	−0.9400	0.088

[a] The exp. values 9888.58 and 11 844.97 were taken from [58].

The results of the predictions of the energy levels for $J = 0$ by these PESs are given in the Tables 2 and 3. These results give information on how well our PESs extrapolate to the higher vibrational energies and what accuracy could be achieved when someone uses these PESs to calculate the line positions for the lines beyond 7000 cm^{-1}.

As the accuracy of our calculations is extraordinary, we decided to present here not only the standard deviations, as in Tables 4 and 5, but also the actual values of discrepancies from the experimentally derived MARVELised (where possible) energy levels for all the levels included in the fit for $J = 0$ (Table 6). The residues (obs-calc) of the $J = 2$ and 5 levels are given in Fig. 1, as well as in the supplementary materials, Table 1. The majority of these values are equal to 0.001 cm^{-1}, which coincides with typical FTS accuracy. These tables give us the opportunity to compare not just the σ values (see Tables 4 and 5) obtained for

Table 4
Summary of our fitted and previous PESs; σ gives the standard deviation from the N experimental levels used in our fits.

PES	σ, cm^{-1}	N
Schröder *ab initio* [59]	1.2520	279
Huang et al. fitted [19]	0.038	279
PES53	0.0089	279
PES60	0.0054	279
PES96	0.0041	279
PES60a	0.0032	251
PES96a	0.0028	250
PES60hJ	0.0050	535

Table 5
Standard deviations for different J levels and different PESs from the MARVEL energy levels. The first line for J values up to 30 corresponds to calculations with PES60, PES96, and PES60hJ potentials and all the MARVEL levels (used in the fit where applicable) included. The second line for each J value corresponds to calculations with PES60a and PES96a potentials in which up to 15% of the worst MARVEL levels were excluded. In the final section, the first line gives a comparison between PES60hJ and Huang et al. line list for MARVEL energies below 11 500 cm^{-1} with $J = 50$; the second line gives a comparison for the set of the best-predicted energies. Hu.ll — Huang et al. line list [19], N — number of levels, σ — standard deviation.

J	PES60/PES60a		Hu.ll		PES96/PES96a		PES60hJ	
	N	σ, cm^{-1}	N	σ, cm^{-1}	N	σ, cm^{-1}	N	σ, cm^{-1}
0	29	0.0067	27	0.0356	29	0.0039	29	0.0061
	26	0.0029			27	0.0023		
2	84	0.0057	76	0.0301	84	0.0040	84	0.0051
	76	0.0032			77	0.0029		
5	99	0.0052	91	0.0277	99	0.0039	99	0.0050
	91	0.0033			93	0.0031		
10	97	0.0051	87	0.0182	97	0.0050	97	0.0046
	87	0.0035			84	0.0034		
15	98	0.0062	88	0.0143	98	0.0078	98	0.0049
	88	0.0049			85	0.0059		
20	100	0.0100	88	0.0284	100	0.0130	100	0.0067
	88	0.0074			85	0.0094		
30	98	0.0190	85	0.0197	98	0.0258	98	0.0119
	85	0.0137			85	0.0204		
50			165	0.160			165	0.051
			86	0.068			86	0.036

the levels presented in the literature, but to do it level by level. Some of those calculated levels coincide with the experiment up to two orders of magnitude better than the accuracy 0.001 cm^{-1} mentioned above.

2.4.1. Extrapolation to higher J levels

Let us consider the results of the extrapolation to higher J levels. As we fitted only the energy levels with $J = 0, 2$ and 5 for the purposes of saving computer time, the results of the extrapolation to higher Js are important from the viewpoint of the accuracy of any subsequent line list. We do not present here the σ of the very high Js needed for the high temperature line lists; however, how well our PESs behave for levels with $J > 5$ which were not included in the fit can be judged from Table 5. Table 5 shows that the extrapolation ($J = 10$, 15 and 20) is excellent and gives results comparable to the σ of the levels used in the fit ($J = 0$, 2 and 5). However, for Js above 20 the extrapolation does start to deteriorate somewhat. This suggests that to achieve an accuracy for very high J levels comparable to that obtained for the lower J levels, we would have to include data on the higher J levels in the fit. The fit of the PES60hJ, which includes the data with Js 10 and 15, is performed in the next section.

The extrapolation of the PES96a's levels to higher Js behaves worse than the one for the PES60 potential, whereas the σ of the lower Js of PES96a is noticeably better. Such behaviour indicates that PES96a represents over-fitting hence the poorer extrapolation properties. This fact demonstrates once again that the further increasing of the number of parameters used to fit the PES would be unproductive, and other methods to further improve the accuracy of the fit should be used.

Thus, we demonstrated in detail the accuracy of the calculated levels both by showing the residues (observed minus calculated values) for particular levels used in the fit (in Tables 2 and 6 and Tables in supplementary materials) and by a detailed analysis of the standard deviations for the fitted levels, for the MARVELized levels only and for higher Js (in Tables 4 and 5). The wavefunctions, corresponding to such levels, on the other hand, demonstrate quite significant instability, as can be seen from the next section, where we analyse the line intensities. The demonstration of such instability is especially seen from the Table 9, where the comparison of multiple calculations is presented. We present the results of intensity calculations using the accurate PESes obtained in this work for completeness. The stability of the wavefunctions generated by these PESs is the subject of the further studies.

2.4.2. Expanding J range

In order to obtain a potential, which would result in an accuracy of about 0.01 cm^{-1} or better for all Js up to $J = 30$, we conducted another refinement of our PES60 by adding 256 extra experimental energy levels with J values equal to 10 and 15 to the dataset we used previously. After a fitting procedure with PES60 taken as a starting point we managed to obtain a new potential PES60hJ, which represents all the 535 available experimental energies up to 7000 cm^{-1} and a bit above with J values 0, 2, 5, 10, and 15 with a standard deviation 0.005 cm^{-1}; Table 4 gives a comparison with all the other potentials, while Table 2 from the Supplementary materials contains the level-by-level list of the corresponding residues.

The accuracy of the new PES60hJ for low-Js is almost the same as for PES60 — 0.0052 cm^{-1} for 279 energy levels with J values 0, 2, and 5. Tables 2 and 3 show deviations of our new results from pure vibrational experimental energies used in the fit which we user to estimate the predictive capabilities of the obtained potentials at higher energies. It can be seen from these tables that, while deviations from energies used in the fit for PES60hJ are close to the ones obtained with PES60, the accuracy of extrapolation to higher energies for PES60hJ is somewhat worse than the one of PES60. That is the price we pay for extending our fits to a wider J range.

Nevertheless, Table 5 shows that our goal is achieved with PES60hJ: extrapolation of the potential to high-J values gives standard deviation 0.007 cm^{-1} for $J = 20$ and 0.01 cm^{-1} for $J = 30$ for the entire reliable set of available MARVEL energy levels, and begins to deteriorate significantly only for $J > 32$. However, even for $J = 50$ the σ value remains quite good, about 0.05 cm^{-1} for almost all the MARVELised energies available, with an exclusion of only 10 outliers, whose residues vary from 0.15 till 1 cm^{-1}. This result is an essential improvement in comparison with PES60 and PES96 potentials. The level-by-level lists of residues, which were used while calculating σ values for PES60hJ, are also presented in the Supplementary material, Tables 3 and 4.

2.4.3. High energy fitted PES

For the fit of the PES to 12 000 cm^{-1} we used the same parameters as for the PES60 fit, gradually increasing the number of coefficients included in the fit from 60 to 96. The standard deviation of the fit was 0.025 cm^{-1}.

Subsequently, we decided to carry out a "Varandisation" [13] of PES60, following the approach we used the water molecule as described in Ref. [63]. All the 637 energy levels up to 12 000 cm^{-1} were fitted. After discarding 10 levels from the fit, the standard deviation became 0.023 cm^{-1}. We call the resulting PES PES12.

The last column of the Table 2 shows the observed minus calculated energy levels for $J = 0$ calculated by the PES12, fitted up to the energies of 12 000 cm^{-1}. The standard deviation of the fitted data up to $J = 5$ is several times worse than our PESes with the limit of energies up to 7000 cm^{-1}. However, these results still demonstrate some improvements over the results published in the literature. The PES12 is also given in the supplementary material.

Table 6
Comparison of levels with $J = 0$ with the experimental levels included in the fit in cm^{-1} for PES96a and Huang et al. line list [19].

exp.	vib.	PES96a	obs. – calc.	Huang.ll	obs. – calc.
1168.1323	0 2 0 0	1168.1317	0.001	1168.133	−0.001
1284.9033	1 0 0 0	1284.9055	−0.002	1284.907	−0.004
2223.7568	0 0 1 0	2223.7572	0.000	2223.762	−0.006
2322.5731	0 4 0 0	2322.5761	−0.003	2322.561	0.012
2461.9964	1 2 0 0	2461.9970	−0.001	2462.031	−0.035
2563.3394	2 0 0 0	2563.3398	0.000	2563.324	0.015
3363.9780	0 2 1 0	3363.9777	0.000	3363.975	0.003
3466.5997	0 6 0 0	3466.5975	0.002	3466.616	−0.016
3480.8192	1 0 1 0	3480.8178	0.001	3480.825	−0.005
3620.9431	1 4 0 0	3620.9433	0.000	3620.921	0.023
3748.2517	2 2 0 0	3748.2549	−0.003	3748.251	0.001
3836.3710	3 0 0 0	3836.3689	0.002	3836.346	0.025
4417.3778	0 0 2 0	4417.3731	0.005	4417.371	0.007
4491.5421	0 4 1 0	4491.5412	0.001	4491.529	0.013
4630.1611	1 2 1 0	4630.1595	0.002	4630.139	0.023
4730.8251	2 0 1 0	4730.8294	−0.004	4730.808	0.017
4767.1421	1 6 0 0	4767.1397	0.002	4767.127	0.015
4910.9955	2 4 0 0	4911.0020	−0.007	4910.974	0.022
5026.3029	3 2 0 0	5026.3062	−0.003	5026.267	0.036
5105.6769	4 0 0 0	5105.6748	0.002	5105.678	−0.001
5529.6950	0 2 2 0	5529.6964	−0.001	5529.660	0.035
5646.7402	1 0 2 0	5646.7316	0.009	5646.734	0.006
5762.3727	1 4 1 0	5762.3730	0.000	5762.315	0.058
5888.1059	2 2 1 0	5888.1104	−0.005	5888.075	0.031
5974.8451	3 0 1 0	5974.8407	0.004	5974.814	0.031
6058.6675	2 6 0 0	6058.6693	−0.002	6058.810	−0.143
6192.2706	3 4 0 0	6192.2720	−0.001	6192.353	−0.083
6295.4476	4 2 0 0	6295.4313	0.016	6295.461	−0.014
6373.3077	5 0 0 0	6373.3095	−0.002	6373.383	−0.075
6580.8537	0 0 3 0	6580.8490	0.005	6580.824	0.030
6768.5017	1 2 2 0	6768.5134	−0.012	6768.446	0.056
6868.5498	2 0 2 0	6868.5404	0.009	6868.518	0.032
7137.1271	3 2 1 0	7137.1229	0.004	7137.092	0.035
7214.6799	4 0 1 0	7214.6761	0.004	7214.675	0.005
7782.6615	1 0 3 0	7782.6581	0.003	7782.654	0.008

3. Intensity calculations

As the Lodi–Tennyson [64] approach for estimating the uncertainty of calculated intensities requires at least two DMSs, we performed our own DMS calculations, which are described in the following subsection.

3.1. Ab initio DMS calculations

As our experience in calculating intensities for HCN [65] and water [66] shows, the external field calculation method (ED) is preferable to the expectation value method (XP) for computing dipole moments. We employed an internally contracted (IC)-MRCI all-electrons method for dipole moment calculations as programmed in MOLPRO [67]. For the dipole moment calculations, we selected the default complete active space (CAS) defined by MRCIC; OCC, 12, 3; CLOSED, 3,0; CORE ,0,0.

Using a cc-pCVQZ-F12 basis proved to be reasonably cheap for the dipole moments calculations, as every dipole point requires 4 independent calculations of the energies in an 0.0003 au external field. We calculated the DMS at about 6000 points. We add a Davidson-fixed correlation correction as well as a relativistic correction, mass–velocity plus first-order Darwin term (MVD1) as produced by MOLPRO.

3.2. Results of intensity calculations using PES60 and two DMSs

Measurements of $^{14}N_2{}^{16}O$ line intensities with sub-percent accuracy are rare; however, two papers providing such measurements have been published recently [49,50]. Comparison of our calculated line intensities with these measurements is given in Tables 7 and 8. and on Figs. 3 and 4: differences are represented as (Obs/Calc−1).

To estimate the accuracy of the intensity calculations using the various PESs plus the DMS obtained here and from the Schröder et al. [59], we calculated intensities for the R4 and R8 lines of the many bands presented in the HITRAN database [22]. The results of these comparisons are given in the Table 9 where the differences are represented as (Obs/Calc−1). The HITRAN database data is mostly based on somewhat less accurate intensity measurements. However, the overall agreement with the all four calculations is excellent. Two types of bands are exceptions from this good agreement. First are bands affected by resonances and the second are bands for which even relatively accurate experimental measurements are not available.

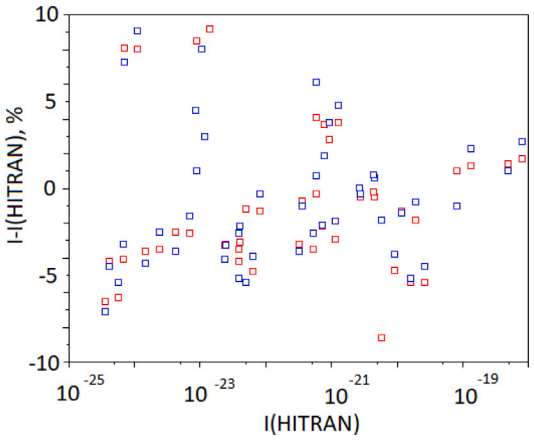

Fig. 3. Differences for 24 bands (see Table 9) between calculated intensities and HITRAN values in percent, blue squares for p60.Sch (PES60 and Schröder et al. DMS [59]) calculation and red squares for PES60.ai (PES60 and *ab initio* DMS).

Table 9 also presents corresponding line intensities taken from Huang et al. [19] for comparison. In some cases our calculations agree worse with the experimental data presented in HITRAN. More accurate measurements are required to produce the final verdict which intensity calculation is actually more accurate.

Table 7
Differences between (42^00) band measured intensities (I in cm/molecule at T = 296 for 100% $^{14}N_2{}^{16}O$) due to Adkins et al. [50] and calculations: Hu.ll — Huang et al. line list [19], PES60.ai — PES60 and our *ab initio* DMS, PES60 and Schröder et al. DMS [59], Yu.ll — line list [20]. The differences in % are given as (Obs/Calc-1)*100.

Line	$\tilde{\omega}$/cm^{-1}	I	Hu.ll	PES60.ai	PES60.Sch	Yu.ll
P10e	6286.473645	2.46E−24	−2.3	−2.8	−4.5	−4.1
P9e	6287.430421	2.29E−24	−3.1	−3.6	−5.3	−4.8
P8e	6288.373997	2.18E−24	0.0	−0.5	−2.3	−1.7
P7e	6289.304378	1.92E−24	−2.6	−3.1	−4.9	−4.3
P6e	6290.221565	1.69E−24	−2.8	−3.3	−5.1	−4.5
P5e	6291.125559	1.45E−24	−2.4	−2.9	−4.6	−4.1
P4e	6292.016361	1.19E−24	−2.0	−2.4	−4.2	−3.7
P3e	6292.893972	9.06E−25	−2.2	−2.6	−4.4	−3.8
P2e	6293.758388	6.03E−25	−3.6	−4.0	−5.8	−5.2
P1e	6294.609609	2.99E−25	−5.3	−5.6	−7.3	−6.7
R0e	6296.272448	3.07E−25	−3.3	−3.6	−5.3	−4.7
R1e	6297.084057	6.22E−25	−1.8	−2.1	−3.9	−3.3
R2e	6297.882451	9.23E−25	−2.1	−2.4	−4.2	−3.6
R3e	6298.667624	1.21E−24	−2.7	−3.0	−4.7	−4.2
R4e	6299.439566	1.50E−24	−2.0	−2.3	−4.0	−3.6
R5e	6300.198270	1.75E−24	−2.9	−3.1	−4.9	−4.4
R6e	6300.943725	2.03E−24	−1.2	−1.4	−3.2	−2.7
R7e	6301.675921	2.23E−24	−2.4	−2.6	−4.4	−3.9
R8e	6302.394846	2.24E−24	−10.1	−10.3	−11.8	−11.5
R9e	6303.100487	2.62E−24	−2.0	−2.2	−3.8	−3.5

Table 8
Differences between (50^00) band measured intensities (I in cm/molecule at T = 296 for 100% $^{14}N_2{}^{16}O$) due to Adkins et al. [50] and calculations: Hu.ll — Huang et al. line list [19], PES60.ai — PES60 and our *ab initio* DMS, PES60 and Schröder et al. DMS [59], H0.ai – Huang [19] PES and our *ab initio* DMS, H0.Sch — Huang et al. PES [19] and Schröder et al. DMS., Yu.ll — line list [20]. The differences in % are given as (Obs/Calc-1)*100.

Line	$\tilde{\omega}$/cm^{-1}	I	Hu.ll	PES60.ai	PES60.Sch	H0.a	H0.Sch	Yu.ll
P10e	6364.329281	1.130E−24	−4.7	8.3	6.0	10.4	8.1	−3.6
P9e	6365.286733	1.080E−24	−3.2	10.0	7.7	12.2	9.8	−2.0
P8e	6366.231001	1.087E−24	5.5	19.8	17.2	22.2	19.6	6.7
P7e	6367.162054	8.929E−25	−4.3	8.6	6.3	10.8	8.5	−3.2
P6e	6368.079869	7.778E−25	−5.7	7.0	4.8	9.2	6.9	−4.6
P5e	6368.984422	6.707E−25	−4.9	7.9	5.6	10.0	7.8	−3.9
P4e	6369.875696	5.485E−25	−4.9	7.9	5.6	10.0	7.8	−3.9
P3e	6370.753673	4.111E−25	−6.6	5.9	3.7	8.0	5.8	−5.6
P2e	6371.618341	2.859E−25	−3.9	8.9	6.7	11.1	8.9	−2.9
P1e	6372.469689	1.434E−25	−4.5	8.3	6.3	10.4	8.3	−3.4
R0e	6374.132400	1.394E−25	−7.7	4.6	2.7	6.6	4.6	−6.7
R1e	6374.943758	2.939E−25	−2.3	10.7	8.5	12.8	10.7	−1.3
R2e	6375.741786	4.242E−25	−5.3	7.3	5.2	9.4	7.4	−4.3
R3e	6376.526487	5.586E−25	−5.3	7.2	5.2	9.3	7.3	−4.3
R4e	6377.297871	6.838E−25	−5.8	6.7	4.7	8.8	6.8	−4.8
R5e	6378.055947	8.121E−25	−4.8	7.8	5.8	9.8	7.9	−3.8
R6e	6378.800729	9.202E−25	−5.2	7.3	5.3	9.3	7.4	−4.3
R7e	6379.532233	1.077E−24	−0.1	13.1	11.0	15.2	13.2	0.9
R8e	6380.250481	1.125E−24	−4.1	8.6	6.6	10.6	8.7	−3.1
R9e	6380.955494	1.202E−24	−4.3	16.0	6.5	10.4	8.4	−3.3

Comparison of intensities for different bands of $^{14}N_2{}^{16}O$ calculated using the same wavefunctions and two different dipole moment (DMS) surfaces shows that for 24 out of 35 bands the obs-calc residues are largely independent of the DMS used. These discrepancies are often very different between Huang et al.'s and our calculations which are performed with different PESs. This suggests that for some bands the most important part of the calculations of line intensity is the accuracy of the wavefunctions and not the accuracy of the DMSs. This is not the case for all the bands. As one can see from the Table 9, the obs-calc residues there depends strongly on the DMS, and significantly more accurate measurements of the line intensities of these bands are needed to better evaluate the DMS (see Fig. 5).

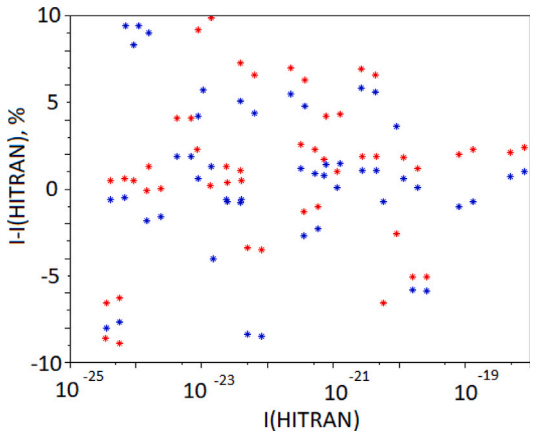

Fig. 4. Differences for 24 bands (see Table 9) between calculated intensities and HITRAN values in percent, blue stars for Hu.Sch (Huang et al. PES [19] and Schröder et al. DMS [59]) and calculation and red stars for Hu.ai (Huang et al. PES [19] and *ab initio* DMS).

4. Conclusion

In this paper we address the long standing problem of computing line positions for a polyatomic molecule using variational calculations with close to the experimental accuracy. We fit experimentally derived energy levels [21] to produce the $^{14}N_2{}^{16}O$ PESs covering energies up to about 7000 cm^{-1}. We obtained the PES of $^{14}N_2{}^{16}O$, which reproduces

Table 9
Differences from effective-dipole moment intensities (I in cm/molecule at $T = 296$ K scaled to 100% $^{14}N_2{}^{16}O$) from HITRAN for strong bands. Calculation with pair PES.DMS (Hu — Huang et al. PES [19], ai — ab initio DMS, Sch — Schröder et al. DMS [59], p60 — PES60, p60.Quad.ai — calculation without quadrature approximation, Yu.ll — line list [20]).

Line	$\tilde{\omega}$	Band	I	Hu.ll	Hu.ai	Hu.Sch	p60.ai	p60.Sch	p60.Quad.ai	Yu.ll
R 4	4.1900	0000	8.394E−24	8.4	57.8	14.6	36.6	2.0	38.0	14.8
R 8	7.5416	0000	4.364E−23	8.1	57.3	14.3	36.2	2.1	37.8	14.5
R 4	1172.3495	0200	2.798E−21	2.8	1.9	1.1	−0.5	−0.3	0.1	−1.5
R 8	1175.7552	0200	4.566E−21	3.0	1.9	1.1	−0.5	−0.3	−0.4	−1.4
R 4	1289.0406	1000	8.313E−20	−3.3	2.0	−1.0	1.0	−1.0	2.1	−0.5
R 8	1292.2870	1000	1.354E−19	−2.9	2.3	−0.7	1.3	−0.8	1.8	−0.3
R 4	2326.8111	0400	2.313E−22	2.7	7.0	5.5	−13.6	−13.9	−17.5	−4.5
R 8	2330.2577	0400	3.737E−22	2.3	6.3	4.8	−14.1	−14.6	−18.0	−5.2
R 4	2466.1605	1200	2.677E−21	3.2	6.9	5.8	0.0	0.0	1.4	5.6
R 8	2469.4599	1200	4.354E−21	3.2	6.6	5.6	−0.2	−0.3	0.6	5.3
R 4	2567.4273	2000	1.202E−20	−0.6	1.8	0.6	−1.3	−1.4	−0.3	0.5
R 8	2570.5747	2000	1.939E−20	−1.1	1.2	0.1	−1.8	−2.1	−0.9	0.0
R 4	3625.1260	1400	3.919E−23	3.8	7.3	5.1	−4.2	−5.2	−5.9	4.1
R 8	3628.4623	1400	6.354E−23	3.3	6.6	4.4	−4.8	−4.9	−6.2	3.4
R 4	3752.3612	2200	3.283E−22	1.6	2.6	1.2	−3.2	−3.6	−1.9	1.1
R 8	3755.5516	2200	5.333E−22	1.4	2.3	0.9	−3.5	−4.0	−2.1	0.7
R 4	3840.4155	3000	7.212E−22	1.6	1.7	0.8	−2.2	−2.1	−1.4	0.2
R 8	3843.4763	3000	1.162E−21	0.9	1.0	0.1	−2.9	−2.9	−2.5	−0.5
R 4	4771.3396	1600	3.566E−25	−10.7	−6.6	−8.0	−6.5	−7.1	1.2	4.5
R 8	4774.7042	1600	5.828E−25	−10.5	−6.3	−7.7	−6.3	−7.1	−0.1	4.6
R 4	4915.1220	2400	4.273E−24	−1.0	4.1	1.9	−2.5	−3.6	−3.8	1.2
R 8	4918.3457	2400	6.970E−24	−1.1	4.1	1.9	−2.6	−3.8	−3.6	1.4
R 4	5030.3546	3200	2.424E−23	−0.3	1.3	−0.6	−3.3	−4.1	−1.8	−1.4
R 8	5033.4295	3200	3.939E−23	−0.6	1.1	−0.8	−3.5	−4.5	−3.1	−1.6
R 4	5109.6882	4000	2.505E−23	−1.6	0.4	−0.7	−3.2	−3.3	−2.9	−2.7
R 8	5112.6830	4000	4.061E−23	−1.5	0.5	−0.6	−3.1	−3.3	−2.7	−2.5
R 4	6196.3380	3400	4.232E−25	−6.0	0.5	−0.6	−4.2	−4.5	−6.2	−3.8
R 8	6199.4436	3400	6.919E−25	−6.0	0.6	−0.5	−4.1	−4.5	−6.1	−2.7
R 4	6299.4395	4200	1.495E−24	−2.4	−0.1	−1.8	−3.6	−4.3	−1.5	−3.9
R 8	6302.3948	4200	2.434E−24	−2.4	0.0	−1.6	−3.5	−4.3	−1.3	−3.8
R 4	6377.2978	5000	7.000E−25	−3.5	11.4	9.4	8.1	7.3	5.6	−2.5
R 8	6380.2504	5000	1.131E−24	−3.6	11.3	9.4	8.0	7.2	4.9	−2.6
R 4	592.9627	0110	5.919E−21	−6.7	−2.8	−0.7	−8.6	−1.8	−7.7	−3.6
R 8	596.32443	0110	9.121E−21	−6.6	1.4	3.6	−4.7	2.3	−4.1	0.5
R 4	1753.2724	0310	1.051E−23	6.4	5.7	4.6	26.7	8.0	28.0	26.2
R 8	1756.6582	0310	1.515E−23	6.9	−4.0	−2.8	14.5	−2.0	13.3	−1.4
R 4	2227.8432	0001	4.929E−19	−2.2	−0.2	0.7	1.4	1.0	2.4	0.8
R 8	2230.9878	0001	8.020E−19	−1.8	0.1	1.0	1.7	0.9	3.1	1.1
R 4	2802.3854	0111	4.889E−22	1.4	−19.1	−17.8	−34.8	−18.4	−34.1	−34.6
R 8	2805.5426	0111	7.333E−22	1.2	−18.2	−17.8	−34.7	−18.3	−33.8	−34.6
R 4	3368.0939	0201	7.980E−22	−2.3	−0.2	1.4	3.7	1.9	4.8	4.6
R 8	3371.2972	0201	1.303E−21	−2.0	−0.1	1.5	3.8	1.9	4.3	4.7
R 4	3484.8524	1001	1.626E−20	−5.0	−6.5	−5.8	−5.4	−5.2	−4.5	−6.5
R 8	3487.8906	1001	2.636E−20	−5.0	−6.6	−5.9	−5.4	−5.4	−4.4	−6.5
R 4	4066.0208	1111	6.232E−24	1.3	57.6	13.6	53.1	12.8	54.9	46.4
R 8	4069.0748	1111	8.960E−24	0.9	43.5	4.2	39.5	3.4	41.8	33.5
R 4	4421.3604	0002	5.828E−22	33.8	20.2	21.8	4.1	6.1	5.7	26.2
R 8	4424.2974	0002	9.404E−22	33.7	18.6	20.3	2.8	4.7	4.4	24.5
R 4	4634.2236	1201	5.091E−23	−9.0	−3.4	−8.4	−1.2	−5.4	0.5	−7.4
R 8	4637.3198	1201	8.273E−23	−9.4	−3.5	−8.5	−1.3	−5.6	0.3	−7.5
R 4	4734.8083	2001	3.606E−22	−4.0	−1.3	−2.7	−0.7	−1.0	0.0	−5.3
R 8	4737.7465	2001	5.869E−22	−3.7	−1.0	−2.3	−0.3	−0.7	0.4	−4.9
R 4	4981.6881	0112	2.232E−24	2.5	−89.8	−73.7	−90.0	−74.0	−89.9	−88.7
R 8	4984.6404	0112	3.333E−24	2.4	−89.9	−73.9	−90.1	−74.2	−90.2	−88.7
R 4	5533.7095	0202	4.273E−25	30.6	870.8	626.8	675.6	492.8	492.2	454.5
R 8	5536.7099	0202	6.970E−25	31.0	843.7	609.2	652.6	477.7	476.5	437.8
R 4	5650.6691	1002	8.556E−24	57.1	2.3	30.5	−16.4	4.5	−13.1	66.5
R 8	5653.4986	1002	1.374E−23	56.3	0.2	27.5	−18.0	−2.1	−14.9	62.6
R 4	5892.1134	2201	3.242E−24	−12.7	−12.6	−18.5	−11.9	−17.1	−9.0	−16.8
R 8	5895.0997	2201	5.293E−24	−12.7	−12.2	−18.2	−11.6	−16.8	−8.5	−16.4
R 4	5978.7849	3001	8.798E−24	−9.0	9.2	0.6	8.5	1.0	7.2	−11.0
R 8	5981.6365	3001	1.434E−23	−8.5	9.9	1.3	9.2	1.7	8.3	−10.4
R 4	6584.7324	0003	1.182E−23	25.7	97.9	16.3	67.8	3.0	65.4	−21.4
R 8	6587.4616	0003	1.909E−23	25.7	94.6	15.0	65.1	1.8	64.5	−22.3
R 4	6872.4284	2002	3.091E−25	−18.4	11 594	138.0	4561.5	104.7	−95.7	−52.6
R 8	6875.1572	2002	5.010E−25	−18.3	11 573	140.0	4545.3	106.1	−94.3	−52.6
R 4	7141.0757	3201	3.545E−25	−10.2	−8.6	−23.1	−10.9	−24.2	−6.3	−20.3
R 8	7143.9444	3201	5.747E−25	−10.7	−8.9	−23.3	−11.2	−24.5	−6.4	−20.6
R 4	7218.5881	4001	3.384E−25	−16.7	133.6	67.8	103.3	50.9	80.5	−24.1
R 8	7221.3766	4001	5.495E−25	−16.5	134.3	68.8	103.8	51.5	81.4	−23.9

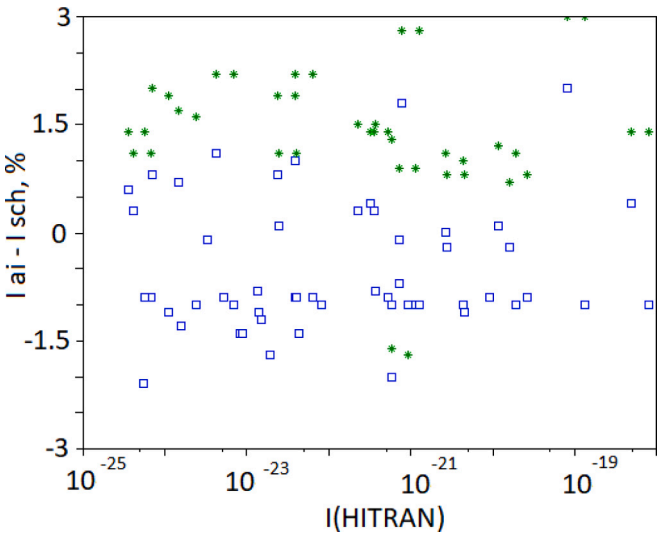

Fig. 5. Differences for 24 bands (see Table 9) between calculated intensities by DMS change from our *ab initio* DMS to the Schröder et al. DMS [59], with PES unchanged, stars for Huang et al. PES [19]: Hu.ai – Hu.Sch difference and squares for PES60: p60.ai – p60.Sch difference.

about 90% of the experimental energy levels within 7000 cm^{-1} range to the accuracy of 0.0028 cm^{-1} and all 100% levels to the slightly worse accuracy of 0.004 cm^{-1}. The standard accuracy of the experimental measurements using Fourier Transform Spectrometers, which are responsible for the majority of infrared (IR) and optical spectra for the most of the molecules, is about 0.002 cm^{-1}. Thus, the accuracy of our calculations has finally become close to the experimental one. Our results pave the way for the attempts to achieve the experimental accuracy of the line positions for the similar triatomic molecules — CO_2 and O_3 [17,41] and provide the solid basis for the accurate variational line list calculation although some adjustments are still necessary to achieve accurate intensities for all bands.

We used these surfaces to calculate the line intensities of $^{14}N_2{}^{16}O$. In order to do that we calculated an *ab initio* DMS using the MRCI level of theory and also used the DMS due to Schröder et al. [59] for comparison. Very accurate line intensities are obtained for both DMSs, as the comparison to the experimentally observed values of line intensities shows. New experimental studies by Gang Li (PTB, private communications, 2024) and others on high accuracy infrared intensities for $^{14}N_2{}^{16}O$ are in progress and we will return to the problem of constructing spectroscopic models which accurately model $^{14}N_2{}^{16}O$ line intensities once these studies are complete.

CRediT authorship contribution statement

Irina I. Mizus: Writing – review & editing, Visualization, Validation, Methodology, Formal analysis. **Mikhail A. Rogov:** Investigation, Formal analysis. **Nikolai F. Zobov:** Validation, Supervision, Methodology, Funding acquisition. **Vladimir Yu. Makhnev:** Methodology, Formal analysis. **Roman I. Ovsyannikov:** Investigation, Formal analysis. **Jonathan Tennyson:** Writing – review & editing, Funding acquisition, Formal analysis. **Oleg L. Polyansky:** Writing – review & editing, Methodology, Investigation, Conceptualization.

Declaration of competing interest

The authors declare no conflict of interest.

Acknowledgements

We acknowledge support by State Project IAP RAS No. FFUF-2024-0016. This work was funded by ERC Advanced Investigator Project 883830. We thank the referees for helpful comments on our original manuscript.

Appendix A. Supplementary data

The supplementary material contains (A) the potential energy surfaces created in this work; (B) full results of the fits in terms of observed minus calculated comparisons.

Supplementary material related to this article can be found online at https://doi.org/10.1016/j.jqsrt.2025.109463.

Data availability

All data are given in the supporting material.

References

[1] Yurchenko SN, Tennyson J, Bailey J, Hollis MDJ, Tinetti G. Spectrum of hot methane in astronomical objects using a comprehensive computed line list. Proc Nat Acad Sci 2014;111:9379–83. http://dx.doi.org/10.1073/pnas.1324219111.

[2] Polyansky OL, Tennyson J. Ab initio calculation of the rotation-vibration energy levels of H_3^+ and its isotopomers to spectroscopic accuracy. J Chem Phys 1999;110:5056–64. http://dx.doi.org/10.1063/1.478404.

[3] Tennyson J, Yurchenko SN. High accuracy molecular line lists for studies of exoplanets and other hot atmospheres. Front Astron Space Sci 2022;8:795040. http://dx.doi.org/10.3389/fspas.2021.795040.

[4] MacDonald JKL. Successive approximations by the Rayleigh–Ritz variation method. Phys Rev 1933;43:830. http://dx.doi.org/10.1103/PhysRev.43.830.

[5] Bubukina II, Zobov NF, Polyansky OL, Shirin SV, Yurchenko SN. Optimized semi-empirical potential energy surface for $H_2{}^{16}O$ up to 26000 cm^{-1}. Opt Spectrosc 2011;110:160–6. http://dx.doi.org/10.1134/S0030400X11020032.

[6] Mizus II, Kyuberis AA, Zobov NF, Makhnev VY, Polyansky OL, Tennyson J. High accuracy water potential energy surface for the calculation of infrared spectra. Philos Trans R Soc Lond A 2018;376:20170149. http://dx.doi.org/10.1098/rsta.2017.0149.

[7] Kostin MA, Polyansky OL, Tennyson J. Calculations of rotation-vibration states with the *z*-axis perpendicular to the plane: high accuracy results for H_3^+. J Chem Phys 2002;116:7564–73.

[8] Jaquet R, Carrington Jr T. Using a nondirect product basis to compute $J > 0$ rovibrational states of H_3^+. J Phys Chem A 2013;117:9493–500. http://dx.doi.org/10.1021/jp312027s.

[9] Sarka J, Poirier B. Assigning quantum labels and improving accuracy for the rovibrational eigenstates of H_3^+ calculated using ScalIT. Front Phys 2022;10:996001. http://dx.doi.org/10.3389/fphy.2022.996001.

[10] Mellau GC, Makhnev VY, Gordon IE, Zobov NF, Tennyson J, Polyansky O. An experimentally-accurate and complete room-temperature infrared HCN line-list for the HITRAN database. J Quant Spectrosc Radiat Transfer 2021;270:107666. http://dx.doi.org/10.1016/j.jqsrt.2021.107666.

[11] Scherrer A, Agostini F, Sebastiani D, Gross EKU, Vuilleumier R. On the mass of atoms in molecules: Beyond the Born–Oppenheimer approximation. Phys Rev X 2017;7:031035. http://dx.doi.org/10.1103/PhysRevX.7.031035.

[12] Partridge H, Schwenke DW. The determination of an accurate isotope dependent potential energy surface for water from extensive ab initio calculations and experimental data. J Chem Phys 1997;106.

[13] Viegas LP, Alijah A, Varandas AJC. Accurate ab initio based multisheeted double many-body expansion potential energy surface for the three lowest electronic singlet states of H_3^+. J Chem Phys 2007;126. http://dx.doi.org/10.1063/1.2566770.

[14] Makhnev VY, Kyuberis AA, Polyansky OL, Mizus II, Tennyson J, Zobov NF. A new spectroscopically-determined potential energy surface and ab initio dipole moment surface for high accuracy HCN intensity calculations. J Mol Spectrosc 2018;353:40–53. http://dx.doi.org/10.1016/j.jms.2018.09.002.

[15] Huang X, Schwenke DW, Tashkun SA, Lee TJ. An isotopic-independent highly accurate potential energy surface for CO_2 isotopologues and an initial $^{12}C^{16}O_2$ infrared line list. J Chem Phys 2012;136:124311. http://dx.doi.org/10.1063/1.1768167.

[16] Huang X, Schwenke DW, Freedman RS, Lee TJ. Ames-2021 CO_2 dipole moment surface and IR line lists: Toward 0.1% uncertainty for CO_2 ir intensities. J Phys Chem A 2022;126:5940–64. http://dx.doi.org/10.1021/acs.jpca.2c01291.

[17] Polyansky OL, Zobov NF, Mizus II, Kyuberis AA, Lodi L, Tennyson J. Potential energy surface, dipole moment surface and the intensity calculations for the 10 μm, 5 μm and 3 μm bands of ozone. J Quant Spectrosc Radiat Transfer 2018;210:127–35. http://dx.doi.org/10.1016/j.jqsrt.2018.02.018.

[18] Tyuterev VG, Kochanov RV, Tashkun SA, Holka F, Szalay PG. New analytical model for the ozone electronic ground state potential surface and accurate *ab initio* vibrational predictions at high energy range. J Chem Phys 2013;139. http://dx.doi.org/10.1063/1.4821638.

[19] Huang X, Schwenke DW, Lee TJ. Highly accurate potential energy surface and dipole moment surface for nitrous oxide and 296 K infrared line list for N_2O. Mol Phys 2023;126. doi:https://huang.seti.org/N2O/n2. in preparation.

[20] Yurchenko SN, Mellor T, Tennyson J. ExoMol line lists – LIX. High-temperature line list for N_2O. Mon Not R Astron Soc 2024;534:1364–75. http://dx.doi.org/10.1093/mnras/stae2201.

[21] Tennyson J, Furtenbacher T, Yurchenko SN, Császár AG. Empirical rovibrational energy levels for nitrous oxide. J Quant Spectrosc Radiat Transfer 2024;316:108902. http://dx.doi.org/10.1016/j.jqsrt.2024.108902.

[22] Gordon IE, Rothman LS, Hargreaves RJ, Hashemi R, Karlovets EV, Skinner FM, Conway EK, Hill C, Kochanov RV, Tan Y, Wcisło P, Finenko AA, Nelson K, Bernath PF, Birk M, Boudon V, Campargue A, Chance KV, Coustenis A, Drouin BJ, Flaud J, Gamache RR, Hodges JT, Jacquemart D, Mlawer EJ, Nikitin AV, Perevalov VI, Rotger M, Tennyson J, Toon GC, Tran H, Tyuterev VG, Adkins EM, Baker A, Barbe A, Canè E, Császár AG, Dudaryonok A, Egorov O, Fleisher AJ, Fleurbaey H, Foltynowicz A, Furtenbacher T, Harrison JJ, Hartmann J, Horneman V, Huang X, Karman T, Karns J, Kassi S, Kleiner I, Kofman V, Kwabia-Tchana F, Lavrentieva NN, Lee TJ, Long DA, Lukashevskaya AA, Lyulin OM, Makhnev VY, Matt W, Massie ST, Melosso M, Mikhailenko SN, Mondelain D, Müller HSP, Naumenko OV, Perrin A, Polyansky OL, Raddaoui E, Raston PL, Reed ZD, Rey M, Richard C, Tóbiás R, Sadiek I, Schwenke DW, Starikova E, Sung K, Tamassia F, Tashkun SA, Vander Auwera J, Vasilenko IA, Vigasin AA, Villanueva GL, Vispoel B, Wagner G, Yachmenev A, Yurchenko SN. The HITRAN2020 molecular spectroscopic database. J Quant Spectrosc Radiat Transfer 2022;277:107949. http://dx.doi.org/10.1016/j.jqsrt.2021.107949.

[23] Tashkun SA, Campargue A. The NOSL-296 high resolution $^{14}N_2\,^{16}O$ line list for atmospheric applications. J Quant Spectrosc Radiat Transfer 2023;295:108417. http://dx.doi.org/10.1016/j.jqsrt.2022.108417.

[24] Tashkun SA, Perevalov VI, Lavrentieva NN. NOSD-1000, the high-temperature nitrous oxide spectroscopic databank. J Quant Spectrosc Radiat Transfer 2016;177:43–8. http://dx.doi.org/10.1016/j.jqsrt.2015.11.014.

[25] Furtenbacher T, Császár AG, Tennyson J. MARVEL: measured active rotational-vibrational energy levels. J Mol Spectrosc 2007;245:115–25.

[26] Zhao X-Q, Wang J, Liu A-W, Zhou Z-Y, Hu S-M. High precision cavity ring down spectroscopy of $6\nu_3$ overtone band of $^{14}N_2^{16}O$ near 775 nm. Chin J Chem Phys 2017;30:487–92. http://dx.doi.org/10.1063/1674-0068/30/cjcp1705109.

[27] Lauzin C, Schmutz H, Agner JA, Merkt F. Chirped-pulse millimetre-wave spectrometer for the 140-180 GHz region. Mol Phys 2018;116:3656–65. http://dx.doi.org/10.1080/00268976.2018.1467055.

[28] AlSaif B, Lamperti M, Gatti D, Laporta P, Fermann M, Farooq A, Lyulin O, Campargue A, Marangoni M. High accuracy line positions of the υ_1 fundamental band of $^{14}N_2\,^{16}O$. J Quant Spectrosc Radiat Transfer 2018;211:172–8. http://dx.doi.org/10.1016/j.jqsrt.2018.03.005.

[29] Liu GL, Wang J, Tan Y, Kang P, Bi Z, Liu AW, Hu SM. Line positions and N_2-induced line parameters of the 00^03 – 00^00 band of $^{14}N_2\,^{16}O$ by comb-assisted cavity ring-down spectroscopy. J Quant Spectrosc Radiat Transfer 2019;229:17–22. http://dx.doi.org/10.1016/j.jqsrt.2019.03.004.

[30] Bertin T, Mondelain D, Karlovets E, Kassi S, Perevalov V, Campargue A. High sensitivity cavity ring down spectroscopy of N_2O near 1.74 μm. J Quant Spectrosc Radiat Transfer 2019;229:40–9. http://dx.doi.org/10.1016/j.jqsrt.2019.02.011.

[31] Zhao G, Bailey DM, Fleisher AJ, Hodges JT, Lehmann KK. Doppler-free two-photon cavity ring-down spectroscopy of a nitrous oxide (N_2O) vibrational overtone transition. Phys Rev A 2020;101:062509. http://dx.doi.org/10.1103/PhysRevA.101.062509.

[32] Karlovets E, Kassi VS, Tashkun SA, Campargue A. The absorption spectrum of nitrous oxide between 8325 and 8622 cm^{-1}. J Quant Spectrosc Radiat Transfer 2021;262:107508. http://dx.doi.org/10.1016/j.jqsrt.2021.107508.

[33] Lucchesini A, Gonzalez-Rivera J. Nitrous oxide spectroscopy at 887 nm. J Quant Spectrosc Radiat Transfer 2022;283:108140. http://dx.doi.org/10.1016/j.jqsrt.2022.108140.

[34] Iwakuni K. Absolute frequency measurement of the $3\nu_1$ band of N_2O with comb-locked rapid scan spectroscopy using a multi-pass cell. J Mol Spectrosc 2022;384:111571. http://dx.doi.org/10.1016/j.jms.2022.111571.

[35] Karlovets EV, Kassi S, Tashkun SA, Campargue A. The absorption spectrum of nitrous oxide between 7647 and 7918 cm^{-1}. J Quant Spectrosc Radiat Transfer 2022;108199. http://dx.doi.org/10.1016/j.jqsrt.2022.108199.

[36] Karlovets EV, Tashkun SA, Kassi S, Campargue A. An improved analysis of the N_2O absorption spectrum in the 1.18 μm window. J Quant Spectrosc Radiat Transfer 2022;278:108003. http://dx.doi.org/10.1016/j.jqsrt.2021.108003.

[37] Hjalten A, Germann M, Krzempek K, Hudzikowski A, Gluszek A, Tomaszewska D, Sobon G, Foltynowicz A. Optical frequency comb Fourier transform spectroscopy of $^{14}N_2\,^{16}O$ at 7.8 μm. J Quant Spectrosc Radiat Transfer 2021;271:107734. http://dx.doi.org/10.1016/j.jqsrt.2021.107734.

[38] Sinitsa LN, Serdyukov VI, Emelyanov NM. Studying the absorption spectra of NNO isotopologues in the region of 4200–6500 cm^{-1}. Russ J Phys Chem A 2024;315:108888. http://dx.doi.org/10.1134/S0036024424700043.

[39] Sinitsa LN, Serdyukov VI, Emelyanov NM, Marinina AA, Perevalov VI. LED-based Fourier transform spectroscopy of $^{14}N_2\,^{16}O$ in the 9750-12000 cm^{-1} region. J Quant Spectrosc Radiat Transfer 2024;315:108888. http://dx.doi.org/10.1016/j.jqsrt.2023.108888.

[40] Sinitsa LN, Vasilchenko SS, Emelyanov NM, Marinina AA, Perevalov VI, Zuev VE. Cavity ring-down spectroscopy of N_2O near 0.83 μm. J Quant Spectrosc Radiat Transfer 2024;329. http://dx.doi.org/10.1016/j.jqsrt.2024.109210.

[41] Polyansky OL, Bielska K, Ghysels M, Lodi L, Zobov NF, Hodges JT, Tennyson J. High accuracy CO_2 line intensities determined from theory and experiment. Phys Rev Lett 2015;114:243001. http://dx.doi.org/10.1103/PhysRevLett.114.243001.

[42] Bielska K, Kyuberis AA, Reed ZD, Li G, Cygan A, Ciuryło R, Adkins EM, Lodi L, Zobov NF, Ebert V, Lisak D, Hodges JT, Tennyson J, Polyansky OL. Subpromille measurements and calculations of CO (3–0) overtone line intensities. Phys Rev Lett 2022;129:043002. http://dx.doi.org/10.1103/PhysRevLett.129.043002.

[43] Guelachvili G, Narahari Rao K. Handbook of infrared standards. San Diego: Academic Press, Inc.; 1986.

[44] Maki AG, Wells JS. New wavenumber calibration tables from heterodyne frequency measurements. J Res Natl Inst Stand Technol 1992;97:409–70.

[45] Morino I, Yamada KMT, Maki AG. Terahertz measurements of rotational transitions in vibrationally excited states of N_2O. J Mol Spectrosc 1999;196:131–8. http://dx.doi.org/10.1006/jmsp.1999.7855.

[46] Horneman V-M. High accurate peak positions for calibration purposes with the lowest fundamental bands ν_2 of N_2O and CO_2. J Mol Spectrosc 2007;241:45–50. http://dx.doi.org/10.1016/j.jms.2006.10.014.

[47] Lepère M, Browet O, Clément J, Vispoel B, Allmendinger P, Hayden J, Eigenmann F, Hugi A, Mangold M. A mid-infrared dual-comb spectrometer in step-sweep mode for high-resolution molecular spectroscopy. J Quant Spectrosc Radiat Transfer 2022;287:108239. http://dx.doi.org/10.1016/j.jqsrt.2022.108239.

[48] Karlovets EV, Mondelain D, Tashkun SA, Campargue A. The absorption spectrum of nitrous oxide between 7250 and 7653 cm^{-1}. J Quant Spectrosc Radiat Transfer 2023;301:108511. http://dx.doi.org/10.1016/j.jqsrt.2023.108511.

[49] Odintsova TA, Fasci E, Gravina S, Gianfrani L, Castrillo A. Optical feedback laser absorption spectroscopy of N_2O at 2 μm. J Quant Spectrosc Radiat Transfer 2020;254:107190. http://dx.doi.org/10.1016/j.jqsrt.2020.107190.

[50] Adkins EM, Long DA, Fleisher AJ, Hodges JT. Near-infrared cavity ring-down spectroscopy measurements of nitrous oxide in the (4200)←(0000) and (5000)←(0000) bands. J Quant Spectrosc Radiat Transfer 2021;262:107527. http://dx.doi.org/10.1016/j.jqsrt.2021.107527.

[51] Karlovets E, Kassi S, Tashkun S, Campargue A. The absorption spectrum of nitrous oxide between 8325 and 8622 cm^{-1}. J Quant Spectrosc Radiat Transfer 2021;262:107508. http://dx.doi.org/10.1016/j.jqsrt.2021.107508.

[52] Karlovets E, Kassi S, Tashkun S, Campargue A. The absorption spectrum of nitrous oxide between 7647 and 7918 cm^{-1}. J Quant Spectrosc Radiat Transfer 2022;288:108199. http://dx.doi.org/10.1016/j.jqsrt.2022.108199.

[53] Vasquez M, Schreier F, Garcia SG, Kitzmann D, Patzer B, Rauer H, Trautmann T. Infrared radiative transfer in atmospheres of earth-like planets around F, G, K, and M stars I. clear-sky thermal emission spectra and weighting functions. Astron Astrophys 2013;549:A26. http://dx.doi.org/10.1051/0004-6361/201219898.

[54] Grenfell JL. A review of exoplanetary biosignatures. Phys Rep 2017;713:1–17. http://dx.doi.org/10.1016/j.physrep.2017.08.003.

[55] Tinetti G, Beaulieu J, Henning T, Meyer M, Micela G, Ribas I, Stam D, Swain M, Krause O, Ollivier M, Pace E, Swinyard B, Aylward A, van Boekel R, Coradini A, Encrenaz T, Snellen I, Zapatero-Osorio MR, Bouwman J, Cho JY-K, Coudé du Foresto V, Guillot T, Lopez-Morales M, Mueller-Wodarg I, Palle E, Selsis F, Sozzetti A, Ade PAR, Achilleos N, Adriani A, Agnor CB, Afonso C, Allende Prieto C, Bakos G, Barber RJ, Barlow M, Batista V, Bernath P, Bézard B, Bordé P, Brown LR, Cassan A, Cavarroc C, Ciaravella A, Cockell C, Coustenis A, Danielski C, Decin L, De Kok R, Demangeon O, Deroo P, Doel P, Drossart P, Fletcher LN, Focardi M, Forget F, Fossey S, Fouqué P, Frith J, Galand M, Gaulme P, González Hernàndez JL, Grasset O, Grassi D, l. Grenfell J, Griffin M, Griffith CA, Grözinger U, Guedel M, Guio P, Hainaut O, Hargreaves R, Hauschildt PH, Heng K, Heyrovsky D, Hueso R, Irwin P, Kaltenegger L, Kervella P, Kipping D, Koskinen TT, Kovács G, La Barbera A, Lammer H, Lellouch E, Leto G, Lopez Morales M, Lopez Valverde MA, Lopez-Puertas M, Lovis C, Maggio A, Maillard JP, Maldonado Prado J, Marquette JB, Martin-Torres F, Maxted P, Miller S, Molinari S, Montes D, Moro-Martin A, Moses JL, Mousis O, Nguyen Tuong N, Nelson R, Orton GS, Pantin E, Pascale E, Pezzuto S, Pinfield D, Poretti E, Prinja R, Prisinzano L, Rees JM, Reiners A, Samuel B, Sánchez-Lavega A, Sanz Forcada J, Sasselov D, Savini G, Sicardy B, Smith A, Stixrude L, Strazzulla G, Tennyson J, Tessenyi M, Vasisht G, Vinatier S, Viti S, Waldmann I, White GJ, Widemann T, Wordsworth R, Yelle R, Yung Y, Yurchenko SN. EChO. Exp Astron 2012;34:311–53.

[56] Tinetti G, Drossart P, Eccleston P, Hartogh P, Heske A, Leconte J, Micela G, Ollivier M, Pilbratt G, Puig L, Turrini D, Vandenbussche B, Wolkenberg P, Beaulieu J-P, Buchave LA, Ferus M, Griffin M, Guedel M, Justtanont K, Lagage P-O, Machado P, Malaguti G, Min M, Nørgaard-Nielsen HU, Rataj M, Ray T, Ribas I,

Swain M, Szabo R, Werner S, Barstow J, Burleigh M, Cho J, du Foresto VC, Coustenis A, Decin L, Encrenaz T, Galand M, Gillon M, Helled R, Morales JC, Muñoz AG, Moneti A, Pagano I, Pascale E, Piccioni G, Pinfield D, Sarkar S, Selsis F, Tennyson J, Triaud A, Venot O, Waldmann I, Waltham D, Wright G, Amiaux J, Auguères J-L, Berthé M, Bezawada N, Bishop G, Bowles N, Coffey D, Colomé J, Crook M, Crouzet P-E, Da Peppo V, Sanz IE, Focardi M, Frericks M, Hunt T, Kohley R, Middleton K, Morgante G, Ottensamer R, Pace E, Pearson C, Stamper R, Symonds K, Rengel M, Renotte E, Ade P, Affer L, Alard C, Allard N, Altieri F, André Y, Arena C, Argyriou I, Aylward A, Baccani C, Bakos G, Banaszkiewicz M, Barlow M, Batista V, Bellucci G, Benatti S, Bernardi P, Bézard B, Blecka M, Bolmont E, Bonfond B, Bonito R, Bonomo AS, Brucato JR, Brun AS, Bryson I, Bujwan W, Casewell S, Charnay B, Pestellini CC, Chen G, Ciaravella A, Claudi R, Clédassou R, Damasso M, Damiano M, Danielski C, Deroo P, Di Giorgio AM, Dominik C, Doublier V, Doyle S, Doyon R, Drummond B, Duong B, Eales S, Edwards B, Farina M, Flaccomio E, Fletcher L, Forget F, Fossey S, Fränz M, Fujii Y, García-Piquer Á, Gear W, Geoffray H, Gérard JC, Gesa L, Gomez H, Graczyk R, Griffith C, Grodent D, Guarcello MG, Gustin J, Hamano K, Hargrave P, Hello Y, Heng K, Herrero E, Hornstrup A, Hubert B, Ida S, Ikoma M, Iro N, Irwin P, Jarchow C, Jaubert J, Jones H, Julien Q, Kameda S, Kerschbaum F, Kervella P, Koskinen T, Krijger M, Krupp N, Lafarga M, Landini F, Lellouch E, Leto G, Luntzer A, Rank-Lüftinger T, Maggio A, Maldonado J, Maillard J-P, Mall U, Marquette J-B, Mathis S, Maxted P, Matsuo T, Medvedev A, Miguel Y, Minier V, Morello G, Mura A, Narita N, Nascimbeni V, Nguyen Tong N, Noce V, Oliva F, Palle E, Palmer P, Pancrazzi M, Papageorgiou A, Parmentier V, Perger M, Petralia A, Pezzuto S, Pierrehumbert R, Pillitteri I, Piotto G, Pisano G, Prisinzano L, Radioti A, Réess J-M, Rezac L, Rocchetto M, Rosich A, Sanna N, Santerne A, Savini G, Scandariato G, Sicardy B, Sierra C, Sindoni G, Skup K, Snellen I, Sobiecki M, Soret L, Sozzetti A, Stiepen A, Strugarek A, Taylor J, Taylor W, Terenzi L, Tessenyi M, Tsiaras A, Tucker C, Valencia D, Vasisht G, Vazan A, Vilardell F, Vinatier S, Viti S, Waters R, Wawer P, Wawrzaszek A, Whitworth A, Yung YL, Yurchenko SN, Osorio MRZ, Zellem R, Zingales T, Zwart F. A chemical survey of exoplanets with ARIEL. Exp Astron 2018;46:135–209. http://dx.doi.org/10.1007/s10686-018-9598-x.

[57] Tennyson J, Kostin MA, Barletta P, Harris GJ, Polyansky OL, Ramanlal J, Zobov NF. DVR3D: a program suite for the calculation of rotation-vibration spectra of triatomic molecules. Comput Phys Comm 2004;163:85–116.

[58] Zuniga J, Alacid M, Bastida A, Requena A. Variational calculations of vibrational states of N_2O using hyperspherical normal coordinates. J Chem Phys 1996;105:6099–110. http://dx.doi.org/10.1063/1.472469.

[59] Schröder B, Sebald P, Stein C, Weser O, Botschwina P. Challenging high-level ab initio rovibrational spectroscopy: The nitrous oxide molecule. Z Phys Chem 2015. http://dx.doi.org/10.1515/zpch-2015-0622.

[60] Yurchenko SN, Carvajal M, Jensen P, Herregodts F, Huet TR. Potential parameters of PH_3 obtained by simultaneous fitting of ab initio data and experimental vibrational band origins. Chem Phys 2003;290:59–67. http://dx.doi.org/10.1016/S0301-0104(03)00098-3.

[61] Henderson JR, Tennyson J, Sutcliffe BT. All the bound vibrational states of H_3^+: a reappraisal. J Chem Phys 1993;98:7191–203.

[62] Partridge H, Schwenke DW. The determination of an accurate isotope dependent potential energy surface for water from extensive *ab initio* calculations and experimental data. J Chem Phys 1997;106:4618–39. http://dx.doi.org/10.1063/1.473987.

[63] Polyansky OL, Kyuberis AA, Zobov NF, Tennyson J, Yurchenko SN, Lodi L. ExoMol molecular line lists XXX: a complete high-accuracy line list for water. Mon Not R Astron Soc 2018;480:2597–608. http://dx.doi.org/10.1093/mnras/sty1877.

[64] Lodi L, Tennyson J. Line lists for $H_2{}^{18}O$ and $H_2{}^{17}O$ based on empirically-adjusted line positions and ab initio intensities. J Quant Spectrosc Radiat Transfer 2012;113:850–8. http://dx.doi.org/10.1016/j.jqsrt.2012.02.023.

[65] Upadhyay A, Conway EK, Tennyson J, Yurchenko SN. ExoMol molecular linelists – XXV: A hot line list for silicon sulphide, SiS. Mon Not R Astron Soc 2018;477:1520–7. http://dx.doi.org/10.1093/mnras/sty998.

[66] Lodi L, Tennyson J. Theoretical methods for small-molecule ro-vibrational spectroscopy. J Phys B: At Mol Opt Phys 2010;43:133001.

[67] Werner H-J, Knowles PJ, Manby FR, Black JA, Doll K, Heßelmann A, Kats D, Köhn A, Korona T, Kreplin DA, Ma Q, Miller TF, Mitrushchenkov A, Peterson KA, Polyak I, Rauhut G, Sibaev M. The molpro quantum chemistry package. J Chem Phys 2020;152(14):144107. http://dx.doi.org/10.1063/5.0005081.